Acta Mech 223, 1323–1340 (2012)
DOI 10.1007/s00707-012-0650-z

Hui Wang · Qing-Hua Qin

A new special element for stress concentration analysis of a plate with elliptical holes

Received: 19 December 2011 / Published online: 7 April 2012

Abstract Special hole elements are presented for analyzing the stress behavior of an isotropic elastic solid containing an elliptical hole. The special hole elements are constructed using the special fundamental solutions for an infinite domain containing a single elliptical hole, which are derived based on complex conformal mapping and Cauchy integrals. During the construction of the special elements, the interior displacement and stress fields are assumed to be the combination of fundamental solutions at a number of source points, and the frame displacement field defined over the element boundary is independently approximated with conventional shape functions. The hybrid finite element model is formulated based on a hybrid functional that provides a link between the two assumed independent fields. Because the fundamental solutions used exactly satisfy both the traction-free boundary conditions of the elliptical hole under consideration and the governing equations of the problems of interest, all integrals can be converted into integrals along the element boundary and there is no need to model the elliptical hole boundary. Thus, the mesh effort near the elliptical hole is significantly reduced. Finally, the numerical model is verified through three examples, and the numerical results obtained for the prediction of stress concentration factors caused by elliptical holes are extremely accurate.

1 Introduction

Stress concentration along the rim of an elliptical hole is important in engineering design. It is of interest, therefore, to consider how to predict the stress concentration factor and stress distribution on the elliptical hole boundary under various loadings as accurately as possible.

Currently, numerical methods are usually used to achieve the desired results for problems associated with one or more elliptical holes under complex boundary constraints and loading conditions. Among them, the conventional finite element method (FEM) has been widely used for such analysis, in which mesh refinement near the elliptical hole is unavoidably required to capture the stress concentration around it and to achieve the necessary numerical accuracy. To address this point, the boundary element method (BEM) using point-force-based fundamental solutions or Green's functions was developed to evaluate the stress concentration factor related to an elliptical hole [1,2], and the BEM using special Green's functions that satisfy the particular boundary conditions is referred to as the special Green's function BEM by Denda [2]. In the special Green's function BEM, the special Green's functions related to the elliptical hole are required to satisfy the proper singularity at the source point and the free boundary conditions along the rim of the elliptical hole.

H. Wang
Institute of Scientific and Engineering Computations, Henan University of Technology, Zhengzhou 450001, People's Republic of China

Q.-H. Qin (✉)
Research School of Engineering, Australian National University, Canberra 0200, Australia
E-mail: qinghua.qin@anu.edu.au

Thus, there is no need for the boundary element to model the elliptical hole. Other contributions to use of the special Green's function BEM for elliptic hole or crack problems in anisotropic media have been made by Clements and Haselgrove [3], Ang and Clements [4], Kamel and Liaw [5], Qin and Mai [6] and Hwu and Liao [7]. However, it is inconvenient to deal with an elastic domain containing multiple elliptical holes using the special Green's function BEM. Moreover, the boundary element alternating method was developed by Ting to treat problems involving multiple elliptical holes in an infinite plane [8].

As an alternative numerical method to the standard FEM and BEM, the hybrid Trefftz finite element method (HT-FEM) in terms of special T-complete solutions related to an elliptical hole for plane elastic media was first established by Piltner [9] to evaluate the stress concentration factor around elliptical holes, without the time-consuming mesh effort around elliptical holes. The advantage of T-complete solutions is that the particular traction-free elliptical hole boundary conditions and the governing equations are automatically satisfied, and thus a large-scale Trefftz element containing an elliptical hole can be constructed to improve the numerical accuracy and simultaneously reduce the mesh effort around the elliptical hole. In the proposed special element, all integrals are evaluated along the element boundary only. Additionally, a formulation that improved on the work of Piltner was proposed by Dhanasekar et al. [10] to provide relatively stable solutions for elliptical hole problems. However, special care must be taken for the derivation and selection of a truncated T-complete solution set for some problems when using HT-FEM, such as the completeness of solutions and the corresponding rigid body motion terms being discarded for the purpose of matrix inversion [11]. Also, to ensure a good numerical condition during the inversion of the matrix, a coordinate transformation is usually required, because the T-complete solutions appearing in the assumed fields may be in the form of a relative higher order of the distance variable.

As an alternative to the HT-FEM, a hybrid finite element formulation based on fundamental solutions has been developed for solving heat transfer problems in isotropic homogeneous solids [12] and fiber-reinforced composites [13], and elastic problems in isotropic [14] and orthotropic [15] media. That numerical model was referred to as HFS-FEM to distinguish it from the HT-FEM, due to the use of fundamental solutions. The present HFS-FEM inherits the advantages of flexible domain element division in the HT-FEM over the conventional FEM and BEM, and avoids some of the shortcomings mentioned above.

In this paper, a special HFS-FEM model is developed to investigate the stress concentration caused by elliptical holes. In the present numerical model, the special fundamental solutions characterizing the local stress effect caused by the interaction of an elliptical hole and concentrated forces are adopted to construct special elliptical-hole elements, in which the proper superposition of fundamental solutions at a number of source points is used to approximate the displacement and stress fields inside the element, while conventional shape functions are employed to interpolate the element boundary displacement field. The hybrid functional at the element level is used to enforce the two assumed fields and to generate the final element stiffness equation. Because the assumed displacement and stress fields inside the element can exactly satisfy both the traction-free boundary conditions and the governing equations, there is no need to model the elliptical hole boundary, and a relatively coarse mesh of the size of the elliptical hole can be employed to discretize the local region of interest. The effort of mesh division near the elliptical hole can then be significantly reduced, while simultaneously the effect of stress concentration along the elliptical hole boundary can be captured more accurately.

This paper is organized as follows. In Sect. 2, the formulations of isotropic elastic problems and the fundamental solutions associated with an elliptical hole are introduced, for the purpose of completeness. Section 3 gives the solution procedure of the present hybrid finite element model, and the special elliptical-hole elements are constructed. Section 4 verifies the proposed numerical model by three examples. The stress concentration for elliptical holes and the interactions between them are investigated using the proposed special elements. In Sect. 5, some conclusions are drawn to summarize the features of this numerical method.

2 Formulations of plane elasticity with elliptical hole

2.1 Governing equations

For a well-posed plane linear elastic problem occupying the domain Ω, the corresponding partial differential governing equations consist of [16]

Equilibrium equations

$$\mathbf{L}\boldsymbol{\sigma} + \mathbf{b} = \mathbf{0}, \tag{1}$$

Strain–displacement relations

$$\boldsymbol{\varepsilon} = \mathbf{L}^{\mathrm{T}}\mathbf{u}, \tag{2}$$

Stress–strain relations

$$\boldsymbol{\sigma} = \mathbf{D}\boldsymbol{\varepsilon}, \tag{3}$$

where $\boldsymbol{\sigma} = \left\{\sigma_{11}\ \sigma_{22}\ \sigma_{12}\right\}^{\mathrm{T}}$ and $\boldsymbol{\varepsilon} = \left\{\varepsilon_{11}\ \varepsilon_{22}\ \gamma_{12}\right\}^{\mathrm{T}}$ denote the stress and strain vectors, respectively, $\mathbf{b} = \left\{b_1\ b_2\right\}^{\mathrm{T}}$ is the body force vector, $\mathbf{u} = \left\{u_1\ u_2\right\}^{\mathrm{T}}$ is the displacement vector, and the differential matrix $\mathbf{L}$ is defined as

$$\mathbf{L} = \begin{bmatrix} \frac{\partial}{\partial x_1} & 0 & \frac{\partial}{\partial x_2} \\ 0 & \frac{\partial}{\partial x_2} & \frac{\partial}{\partial x_1} \end{bmatrix}, \tag{4}$$

and x_i $(i = 1, 2)$ are the global Cartesian coordinates. The stress–strain matrix $\mathbf{D}$ is given by

$$\mathbf{D} = \frac{E^*}{1-\nu^{*2}} \begin{bmatrix} 1 & \nu^* & 0 \\ \nu^* & 1 & 0 \\ 0 & 0 & \frac{1-\nu^*}{2} \end{bmatrix}, \tag{5}$$

with $E^* = E$, $\nu^* = \nu$ for plane stress analysis and $E^* = E/(1-\nu^2)$, $\nu^* = \nu/(1-\nu)$ for plane strain analysis. E and ν, respectively, denote the elastic modulus and the Poisson's ratio.

As well, the specified boundary displacement and traction conditions should be complemented, such as

$$\left.\begin{array}{ll} \mathbf{u} = \bar{\mathbf{u}} & \text{on } \Gamma_u \\ \mathbf{s} = \mathbf{A}\boldsymbol{\sigma} = \bar{\mathbf{s}} & \text{on } \Gamma_s \end{array}\right\}, \tag{6}$$

where an overbar represents a specified variable, and

$$[\mathbf{A}] = \begin{bmatrix} n_1 & 0 & n_2 \\ 0 & n_2 & n_1 \end{bmatrix}, \tag{7}$$

where n_i represents the ith component of the outward normal to the boundary

$$\Gamma = \Gamma_u + \Gamma_s.$$

Rearranging Eq. (3) leads to the following Cauchy–Navier equations in terms of displacements:

$$\mathbf{L}\mathbf{D}\mathbf{L}^{\mathrm{T}}\mathbf{u} + \mathbf{b} = \mathbf{0}. \tag{8}$$

2.2 Fundamental solutions for an elliptical hole

In the process of constructing special elliptical-hole elements for stress concentration analysis in the next section, the key step is to find proper fundamental solutions that reflect the local stress concentration attributable to an elliptical hole. To achieve this, the interaction of an elliptical hole and a concentrated load in an infinite elastic medium is considered, here using Muskhelishvili's complex variable formulation [17].

When a concentrated point force $F = F_1 + F_2 i$ is applied at the point $z_0 = x_1^s + x_2^s i$ outside an elliptical hole with major and minor axes $a, b(a \geq b)$ along the x_1, x_2 axes at the origin (see Fig. 1), the induced displacements and stresses solutions can be obtained using complex elastic theory, that is, the displacements and stresses in the isotropic elastic medium can be expressed through two complex functions $\psi_1(z), \varphi_1(z)$, such that [17]

$$2G(u_1 + u_2 i) = \kappa\psi_1(z) - z\overline{\psi_1'(z)} - \overline{\varphi_1(z)} \tag{9}$$

and

$$\begin{aligned} \sigma_{11} + \sigma_{22} &= 2\left[\psi_1'(z) + \overline{\psi_1'(z)}\right], \\ \sigma_{22} - \sigma_{11} + 2\sigma_{12} i &= 2\left\{\bar{z}\psi_1''(z) + \varphi_1'(z)\right\}, \end{aligned} \tag{10}$$

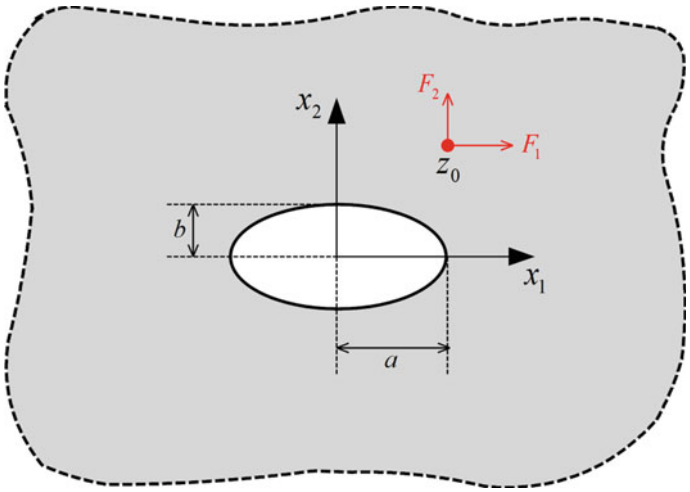

Fig. 1 Infinite plane with an *elliptical hole* under concentrated forces

where $i = \sqrt{-1}$, $\kappa = 3-4\nu$ for plane strain and $\kappa = (3-\nu)/(1+\nu)$ for plane stress. A bar over a complex variable indicates its conjugate and a prime denotes differentiation with respect to the independent variable, i.e.,

$$\psi_1'(z) = \frac{\mathrm{d}\psi_1(z)}{\mathrm{d}z}, \quad \psi_1''(z) = \frac{\mathrm{d}^2\psi_1(z)}{\mathrm{d}z^2}, \quad \varphi_1'(z) = \frac{\mathrm{d}\varphi_1(z)}{\mathrm{d}z}. \tag{11}$$

Also, we have the following expression for the resultant forces P_1, P_2 on an arc AB of the boundary from point A to point B:

$$-i\,(P_1 - P_2 i) = \left[\overline{\psi_1(z)} + \bar{z}\psi_1'(z) + \varphi_1(z)\right]_A^B. \tag{12}$$

To convert the elliptical hole into a unit circle, the following conformal mapping is defined:

$$z = z(w) = R\left(w + \frac{m}{w}\right), \tag{13}$$

where the parameters R and m are related to the major and minor axes by

$$R = \frac{1}{2}(a+b), \quad m = \frac{a-b}{a+b}. \tag{14}$$

The mapping function (13) maps the ellipse onto a unit circle (see Fig. 2) and also maps the exterior of the ellipse onto the exterior of a unit circle. Based on this consideration, the inverse mapping function is given by

$$w = \frac{z + \sqrt{z^2 - 4R^2 m}}{2R}, \tag{15}$$

when the real part of the complex variable z is larger than zero or z is located at the positive axes of the coordinate system, and

$$w = \frac{z - \sqrt{z^2 - 4R^2 m}}{2R}, \tag{16}$$

when the real part of the complex number z is less than zero or z is located at the negative axes of the coordinate system.

For the interaction of the pair of point forces F and an elliptical hole, Eq. (13) maps the elliptical hole in the z-plane onto a unit circle at the origin of the w-plane, and the points z and z_0 in the z-plane onto points w and w_0 in the w-plane.

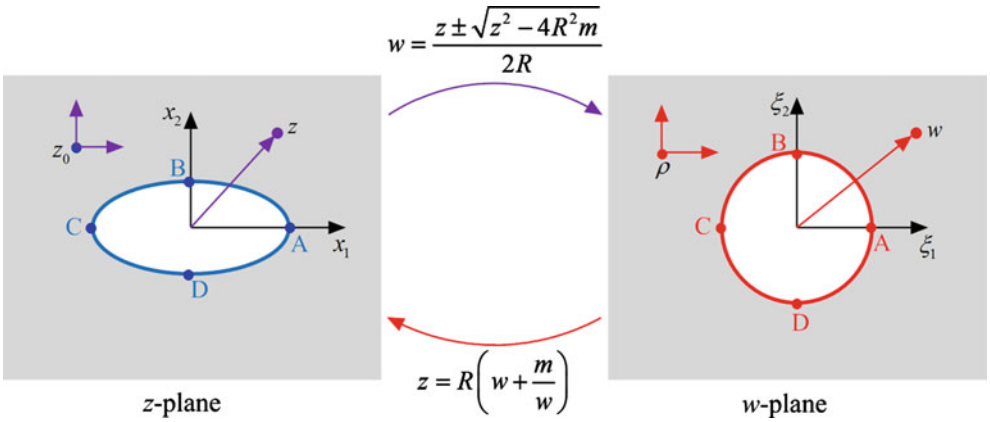

Fig. 2 Conformal mapping of an infinite plane with an *elliptical hole*

Now the complex potentials defined in the actual domain (z-plane) are transformed into functions of w through the relations

$$\psi_1(z) = \psi_1(z(w)) = \psi(w), \quad \varphi_1(z) = \varphi_1(z(w)) = \varphi(w). \tag{17}$$

It is obvious that if the elasticity solution is known for the geometry in the w-plane, then through appropriate inverse transformation formulae the solution for the actual problem can be determined.

Because the sought complex potential functions are expressed in the transformed domain, that is, $\psi(w)$, $\varphi(w)$, the following relations are useful for distinguishing those derivatives respectively defined in different spaces, for example,

$$\begin{aligned} \psi_1'(z) &= \frac{\mathrm{d}\psi_1(z)}{\mathrm{d}z}, \qquad \dot{\psi}(w) = \frac{\mathrm{d}\psi(w)}{\mathrm{d}w}, \\ \psi_1''(z) &= \frac{\mathrm{d}^2\psi_1(z)}{\mathrm{d}z^2}, \qquad \ddot{\psi}(w) = \frac{\mathrm{d}^2\psi(w)}{\mathrm{d}w^2}, \\ \varphi_1'(z) &= \frac{\mathrm{d}\varphi_1(z)}{\mathrm{d}z}, \qquad \dot{\varphi}(w) = \frac{\mathrm{d}\varphi(w)}{\mathrm{d}w}. \end{aligned} \tag{18}$$

Using the chain rule of derivatives, we have

$$\begin{aligned} \psi_1'(z) &= \dot{\psi}(w)\frac{\mathrm{d}w}{\mathrm{d}z} = \frac{\dot{\psi}(w)}{\dot{z}(w)}, \\ \psi_1''(z) &= \frac{\ddot{\psi}(w)}{[\dot{z}(w)]^2} - \dot{\psi}(w)\frac{\ddot{z}(w)}{[\dot{z}(w)]^3} \end{aligned} \tag{19}$$

and

$$\varphi_1'(z) = \dot{\varphi}(w)\frac{\mathrm{d}w}{\mathrm{d}z} = \frac{\dot{\varphi}(w)}{\dot{z}(w)}. \tag{20}$$

As a result, Eqs. (9), (10), and (12) can be rewritten in the transformed space as

$$\begin{aligned} 2G(u_1 + u_2 i) &= \kappa\psi(w) - z(w)\overline{\frac{\dot{\psi}(w)}{\dot{z}(w)}} - \overline{\varphi(w)}, \\ \sigma_{11} + \sigma_{22} &= 4Re\left[\frac{\dot{\psi}(w)}{\dot{z}(w)}\right], \\ \sigma_{22} - \sigma_{11} + 2\sigma_{12} i &= 2\left\{\overline{z(w)}\left(\frac{\ddot{\psi}(w)}{[\dot{z}(w)]^2} - \dot{\psi}(w)\frac{\ddot{z}(w)}{[\dot{z}(w)]^3}\right) + \frac{\dot{\varphi}(w)}{\dot{z}(w)}\right\}, \\ -i\,(P_1 - P_2 i) &= \left[\overline{\psi(w)} + \overline{z(w)}\frac{\dot{\psi}(w)}{\dot{z}(w)} + \varphi(w)\right]_A^B. \end{aligned} \tag{21}$$

Using the complex variable formalism of Muskhelishvili, Green's function solutions for the hole problem can be written in the form [2]

$$\begin{aligned} \psi(w) &= \psi_s(w) + \psi_r(w), \\ \varphi(w) &= \varphi_s(w) + \varphi_r(w), \end{aligned} \tag{22}$$

where $\psi_s(w)$ and $\varphi_s(w)$ are the singular parts for an infinite body subjected to an concentrated force and containing no hole or other defects; $\psi_r(w)$ and $\varphi_r(w)$ are the regular parts to be determined so that the traction on the surface of the hole becomes zero.

According to complex elastic theory, the singular parts in the w-plane can be given by

$$\begin{aligned} \phi_s(w) &= -\gamma \ln\left[z(w) - z(\rho)\right], \\ \psi_s(w) &= \kappa\bar{\gamma} \ln\left[z(w) - z(\rho)\right] + \gamma \frac{\overline{z(\rho)}}{z(w) - z(\rho)}, \end{aligned} \tag{23}$$

where

$$\gamma = \frac{F_1 + F_2 i}{2\pi(1+\kappa)}. \tag{24}$$

With the help of Cauchy integrals, the resulting regular terms can be given by [2]

$$\begin{aligned} \psi_r(w) &= \psi_{r1}(w)\gamma + \psi_{r2}(w)\bar{\gamma}, \\ \varphi_r(w) &= \varphi_{r1}(w)\gamma + \varphi_{r2}(w)\bar{\gamma} - \frac{z\left(\frac{1}{w}\right)}{z'(w)}\psi_r'(w), \end{aligned} \tag{25}$$

where

$$\begin{aligned} \psi_{r1}(w) &= \ln\left(1 - \frac{m}{w\rho}\right) - \kappa \ln\left(1 - \frac{1}{w\bar{\rho}}\right), \\ \psi_{r2}(w) &= \frac{\rho(1 + m\bar{\rho}^2) - \bar{\rho}(m + \rho^2)}{\rho(m - \bar{\rho}^2)} \frac{1}{\bar{\rho}w - 1}, \\ \varphi_{r1}(w) &= \frac{\bar{\rho}(m^3 + \rho^2) - m\rho(m + \bar{\rho}^2)}{\bar{\rho}(m - \rho^2)} \frac{1}{\rho w - m}, \\ \varphi_{r2}(w) &= -\kappa \ln\left(1 - \frac{m}{w\rho}\right) + \ln\left(1 - \frac{1}{w\bar{\rho}}\right). \end{aligned} \tag{26}$$

2.3 Coordinate transformation for an inclined elliptical hole

If the semi-axes of the ellipse are along, for example, the coordinate axes of the local system $(\hat{x}_1, \hat{x}_2)$ rather than those of the global system (x_1, x_2), then a coordinate transformation is needed during the derivation of the hybrid finite element model with special elements in this study.

For the two coordinate systems mentioned above with same origin (see Fig. 3), the angle between the two axes is denoted by an angle θ, which is positive in the anti-clockwise direction. Then the global and local coordinates are related to each other through the angle θ:

$$\begin{Bmatrix} x_1 \\ x_2 \end{Bmatrix} = \mathbf{T}_1^{-1} \begin{Bmatrix} \hat{x}_1 \\ \hat{x}_2 \end{Bmatrix} \tag{27}$$

or

$$\begin{Bmatrix} \hat{x}_1 \\ \hat{x}_2 \end{Bmatrix} = \mathbf{T}_1 \begin{Bmatrix} x_1 \\ x_2 \end{Bmatrix} \tag{28}$$

where $\mathbf{T}_1$ is called the transformation matrix and is defined as

$$\mathbf{T}_1 = \begin{bmatrix} c & s \\ -s & c \end{bmatrix} \tag{29}$$

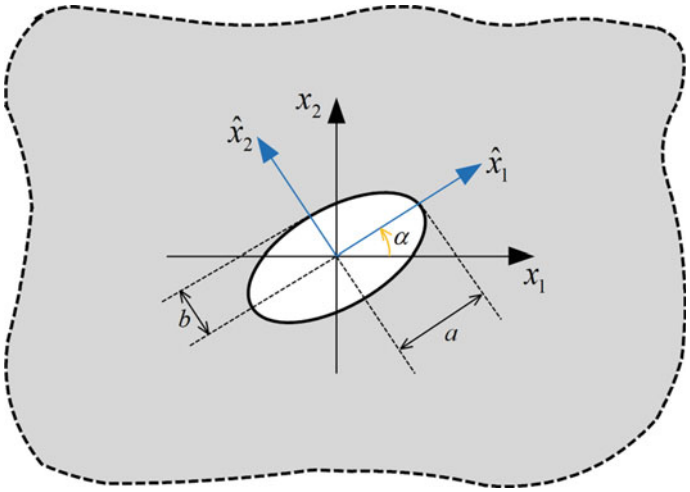

Fig. 3 Global and local coordinate systems defined for an inclined *elliptical hole*

or its inverse matrix

$$\mathbf{T}_1^{-1} = \begin{bmatrix} c & -s \\ s & c \end{bmatrix} \tag{30}$$

with $c = \cos(\theta)$, $s = \sin(\theta)$.

Subsequently, for the inclined elliptical hole, the relationship for transformation of displacement and stress components between the local and global coordinate systems is given by

$$\begin{Bmatrix} u_1 \\ u_2 \end{Bmatrix} = \mathbf{T}_1^{-1} \begin{Bmatrix} \hat{u}_1 \\ \hat{u}_2 \end{Bmatrix}, \tag{31}$$

$$\begin{Bmatrix} \sigma_{11} \\ \sigma_{22} \\ \sigma_{12} \end{Bmatrix} = \mathbf{T}_2^{-1} \begin{Bmatrix} \hat{\sigma}_{11} \\ \hat{\sigma}_{22} \\ \hat{\sigma}_{12} \end{Bmatrix}, \tag{32}$$

where the stress transformation matrix $\mathbf{T}_2$ is defined as

$$\mathbf{T}_2 = \begin{bmatrix} c^2 & s^2 & 2cs \\ s^2 & c^2 & -2cs \\ -cs & cs & c^2 - s^2 \end{bmatrix}, \tag{33}$$

or its inverse matrix

$$\mathbf{T}_2^{-1} = \begin{bmatrix} c^2 & s^2 & -2cs \\ s^2 & c^2 & 2cs \\ cs & -cs & c^2 - s^2 \end{bmatrix}. \tag{34}$$

3 Development of HFS finite element formulation

3.1 Element interior fields

In the absence of body forces, motivated by the basic idea of the method of fundamental solution (MFS) [18] to remove the singularity of a fundamental solution, for a particular element e, which occupies a sub-domain Ω_e, we first assume that the field variable defined in the element domain is extracted from a linear combination of fundamental solutions centered at different source points, that is,

$$\mathbf{u}_e = \mathbf{N}\mathbf{c}_e, \tag{35}$$

where $\mathbf{c}_e = \left[c_{11}\ c_{21}\ \cdots\ c_{1n_s}\ c_{2n_s} \right]^{\mathrm{T}}$ is an unknown coefficient vector (not a nodal displacement vector) consisting of the source intensity at n_s source points outside the element domain, and the coefficient matrix

$$\mathbf{N} = \begin{bmatrix} u^*_{11}(\mathbf{x}, \mathbf{y}_1)\ u^*_{21}(\mathbf{x}, \mathbf{y}_1) \cdots u^*_{11}\left(\mathbf{x}, \mathbf{y}_{n_s}\right)\ u^*_{21}\left(\mathbf{x}, \mathbf{y}_{n_s}\right) \\ u^*_{12}(\mathbf{x}, \mathbf{y}_1)\ u^*_{22}(\mathbf{x}, \mathbf{y}_1) \cdots u^*_{12}\left(\mathbf{x}, \mathbf{y}_{n_s}\right)\ u^*_{22}\left(\mathbf{x}, \mathbf{y}_{n_s}\right) \end{bmatrix},$$

consists of the fundamental solution $u^*_{li}\left(\mathbf{x}, \mathbf{y}_j\right)$, $\mathbf{x}$ and $\mathbf{y}_j$ are field point and source point measured in the local coordinate system (x_1, x_2), respectively.

In practice, the generation of virtual sources outside the element domain can usually be achieved by means of the following formulation [12,19,20]

$$\mathbf{y}_j = \mathbf{x}_b + \gamma\left(\mathbf{x}_b - \mathbf{x}_c\right), \tag{36}$$

where γ is a dimensionless coefficient, $\mathbf{x}_b$ is the elementary boundary point and $\mathbf{x}_c$ the geometrical centroid of the element. Typically, in the proposed approach, we use the nodes of the element to generate related source points for simplicity.

Subsequently, differentiating Eq. (35), we obtain the corresponding stress fields

$$\boldsymbol{\sigma}_e = \mathbf{T}\mathbf{c}_e \tag{37}$$

with

$$\mathbf{T} = \begin{bmatrix} \sigma^*_{111}(\mathbf{x}, \mathbf{y}_1)\ \sigma^*_{211}(\mathbf{x}, \mathbf{y}_1) \cdots \sigma^*_{111}\left(\mathbf{x}, \mathbf{y}_{n_s}\right)\ \sigma^*_{211}\left(\mathbf{x}, \mathbf{y}_{n_s}\right) \\ \sigma^*_{122}(\mathbf{x}, \mathbf{y}_1)\ \sigma^*_{222}(\mathbf{x}, \mathbf{y}_1) \cdots \sigma^*_{122}\left(\mathbf{x}, \mathbf{y}_{n_s}\right)\ \sigma^*_{222}\left(\mathbf{x}, \mathbf{y}_{n_s}\right) \\ \sigma^*_{112}(\mathbf{x}, \mathbf{y}_1)\ \sigma^*_{212}(\mathbf{x}, \mathbf{y}_1) \cdots \sigma^*_{112}\left(\mathbf{x}, \mathbf{y}_{n_s}\right)\ \sigma^*_{212}\left(\mathbf{x}, \mathbf{y}_{n_s}\right) \end{bmatrix},$$

Furthermore, the boundary traction vector $\mathbf{s}$ is evaluated by

$$\mathbf{s}_e = \mathbf{Q}\mathbf{c}_e, \tag{38}$$

where

$$\mathbf{Q} = \mathbf{A}\mathbf{T}. \tag{39}$$

3.2 Element frame field

To enforce conformity on the displacement field over the interface of two neighboring elements e and f, for instance, $\mathbf{u}_e = \mathbf{u}_f$ on $\Gamma_e \cap \Gamma_f$, an auxiliary inter-element frame field $\tilde{\mathbf{u}}_e$ defined along the element boundary is assumed in terms of the nodal degrees of freedom (DOF) $\mathbf{d}_e$, that is,

$$\tilde{\mathbf{u}}_e = \tilde{\mathbf{N}}\mathbf{d}_e, \tag{40}$$

in which the matrix $\tilde{\mathbf{N}}$ is formed with respect to shape functions used in the standard FEM and BEM.

3.3 Hybrid functional and stiffness equation

Having independently defined the intra-element field and frame field in a particular element e, the hybrid functional Π_{me} in the absence of body forces is given by [21]

$$\Pi_{me} = \frac{1}{2}\int_{\Omega_e} \boldsymbol{\sigma}^{\mathrm{T}}\boldsymbol{\varepsilon}\,\mathrm{d}\Omega - \int_{\Gamma_e^s} \bar{\mathbf{s}}^{\mathrm{T}}\tilde{\mathbf{u}}\,\mathrm{d}\Gamma + \int_{\Gamma_e} \mathbf{s}^{\mathrm{T}}\left(\tilde{\mathbf{u}} - \mathbf{u}\right)\,\mathrm{d}\Gamma, \tag{41}$$

which can be used to link the two independent fields and to generate the element stiffness equation.

Applying the Gaussian theorem again to the above hybrid functional, we have

$$\Pi_{me} = -\frac{1}{2}\int_{\Gamma_e} \mathbf{u}^{\mathrm{T}}\mathbf{s}\,\mathrm{d}\Gamma - \int_{\Gamma_e^s} \bar{\mathbf{s}}^{\mathrm{T}}\tilde{\mathbf{u}}\,\mathrm{d}\Gamma + \int_{\Gamma_e} \mathbf{s}^{\mathrm{T}}\tilde{\mathbf{u}}\,\mathrm{d}\Gamma, \tag{42}$$

Substituting Eqs. (35), (38) and (40) into the functional (42) yields

$$\Pi_{me} = -\frac{1}{2}\mathbf{c}_e^{\mathrm{T}}\mathbf{H}_e\mathbf{c}_e - \mathbf{d}_e^{\mathrm{T}}\mathbf{g}_e + \mathbf{c}_e^{\mathrm{T}}\mathbf{G}_e\mathbf{d}_e, \tag{43}$$

in which

$$\mathbf{H}_e = \int_{\Gamma_e} \mathbf{Q}^{\mathrm{T}}\mathbf{N}\,\mathrm{d}\Gamma, \quad \mathbf{G}_e = \int_{\Gamma_e} \mathbf{Q}^{\mathrm{T}}\tilde{\mathbf{N}}\,\mathrm{d}\Gamma, \quad \mathbf{g}_e = \int_{\Gamma_e^s} \tilde{\mathbf{N}}^{\mathrm{T}}\bar{\mathbf{s}}\,\mathrm{d}\Gamma. \tag{44}$$

To enforce inter-element continuity on the common element boundary, the unknown vector $\mathbf{c}_e$ should be expressed in terms of the nodal DOFs$\mathbf{d}_e$. Minimization of the functional Π_{me} with respect to $\mathbf{c}_e$ and $\mathbf{d}_e$, respectively, yields

$$\begin{aligned} \frac{\partial \Pi_{me}}{\partial \mathbf{c}_e^{\mathrm{T}}} &= -\mathbf{H}_e\mathbf{c}_e + \mathbf{G}_e\mathbf{d}_e = \mathbf{0}, \\ \frac{\partial \Pi_{me}}{\partial \mathbf{d}_e^{\mathrm{T}}} &= \mathbf{G}_e^{\mathrm{T}}\mathbf{c}_e - \mathbf{g}_e = \mathbf{0}, \end{aligned} \tag{45}$$

from which the optional relationship between $\mathbf{c}_e$ and $\mathbf{d}_e$, and the stiffness equation can be produced, that is,

$$\mathbf{c}_e = \mathbf{H}_e^{-1}\mathbf{G}_e\mathbf{d}_e \tag{46}$$

and

$$\mathbf{K}_e\mathbf{d}_e = \mathbf{g}_e, \tag{47}$$

where

$$\mathbf{K}_e = \mathbf{G}_e^{\mathrm{T}}\mathbf{H}_e^{-1}\mathbf{G}_e \tag{48}$$

stands for the element stiffness matrix, which is symmetric and can be easily incorporated into the standard finite element program.

3.4 Special elliptical-hole element

From the hybrid formulation described above, we can see that the independence of the interior and boundary fields for a particular element makes it possible to construct arbitrarily shaped hybrid elements, such as elements with more edges and nodes. More importantly, because the assumed interior fields analytically satisfy the governing equations and the local boundary condition associated with an elliptical hole within the element domain, it is reasonable to design a special large-scale element to enclose the elliptical hole with multiple edges and nodes. In general, the interpolation functions provide more accurate solutions when the number of source points is increased. However, the solutions may become unstable in practice when more source points are chosen, because the induced larger order of the matrix $\mathbf{H}_e$ may decrease the numerical accuracy of its inverse manipulation. Here, two types of special element are designed: One is an 8-node special element and the other a 16-node special element. These elements are constructed with quadratically varying frame displacements as shown in Fig. 4.

4 Numerical results

To assess the performance of the proposed approach and the associated special elements, three numerical examples are considered in this section. The first example is considered for validating the present special element by comparing numerical results with available analytical solutions. The second example is used to assess the behavior of the special element for solving an inclined elliptical hole. The final numerical experiment is used to assess the ability of the present special element for simulating the interaction between two elliptical holes.

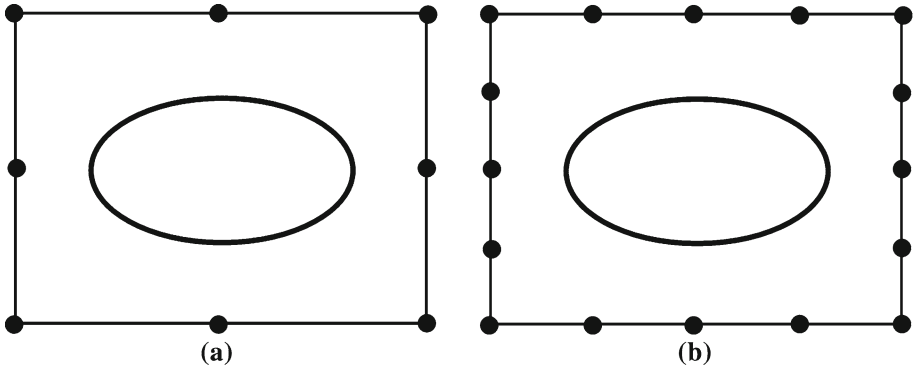

Fig. 4 Special *elliptical-hole* elements with **a** 8 nodes, **b** 16 nodes

4.1 Infinite plate with a centered elliptical hole under tension

The first example, for which exact solutions are available, is chosen to demonstrate the accuracy of the present special elliptical-hole element. In this example, we analyze an infinite plate with a centered elliptical hole subjected to unidirectional tension, and the plane stress state is assumed. The exact complex potential solutions for such case can be determined by using Cauchy integral methods, as found in Muskhelishvili [17]:

$$\begin{aligned} \psi(w) &= \frac{pR}{4}\left(w - \frac{2+m}{w}\right), \\ \varphi(w) &= -\frac{pR}{2}\left(-w - \frac{1}{mw} - \frac{\left(1+m^2\right)(-1-m)}{m}\frac{w}{w^2-m}\right). \end{aligned} \tag{49}$$

The related stress concentration factor (SCF) on the hoop stress σ_θ at the top point $(a, 0)$ of the elliptical boundary is given by

$$\frac{(\sigma_\theta)_{\max}}{p} = 1 + 2\frac{a}{b}. \tag{50}$$

In the computation, the infinite domain is idealized by a large square domain taken from the work of Piltner [22] with the side length 100, and the major axis of the elliptical hole is taken to be $a = 2$, as shown in Fig. 5. The applied uniform tension load p is assumed to be 1. The mesh configuration associated with one 8-node special hybrid element and 48 8-node general hybrid elements is displayed in Fig. 6. The total number of nodes is 176. Four symmetric displacement constraints at points $(\pm 50, 0)$, $(0, \pm 50)$ are imposed during the computation. The effect of the location of source points on the stress concentration of hoop stress is first investigated for the case of $a/b = 2$, and the numerical results displayed in Fig. 7 show that stable results can be achieved for a large range of values of the parameter γ. It is found that with too small a value of γ the source points are too close to the physical boundary of the hybrid element, leading to vibrating results due to the near singularity of fundamental solutions. However, when the source points are remote from the element physical boundary, the numerical accuracy can decrease due to the round-off error caused by the large magnitude difference between the unknown interpolating coefficient $\mathbf{c}_e$ and nodal displacement $\mathbf{d}_e$. Hence, $\gamma = 5$ is chosen in the subsequent computation, and a similar suggestion can be found in the authors' previous work [12,14,15]. Next, the corresponding variation of hoop stress along the elliptical hole boundary is displayed in Fig. 8, and it is seen that there is good agreement between the numerical results using the present hybrid finite element model and the analytical solutions. As well, the decays of stress components σ_{11} and σ_{22} away from the edge of the elliptical hole are shown in Figs. 9 and 10, from which it can be seen that the magnitude of the stress components decays rapidly to the state without the elliptical hole, so the correctness of the truncated size of the infinite plate is illustrated.

Finally, the stress concentration factor for various ratios of a/b is calculated, and numerical and analytical solutions are tabulated in Table 1, from which it is found that the maximum relative error is just 0.27 %, indicating that the present hybrid model can accurately capture the dramatic variation of stress on the elliptical hole boundary and the constructed special element is verified.

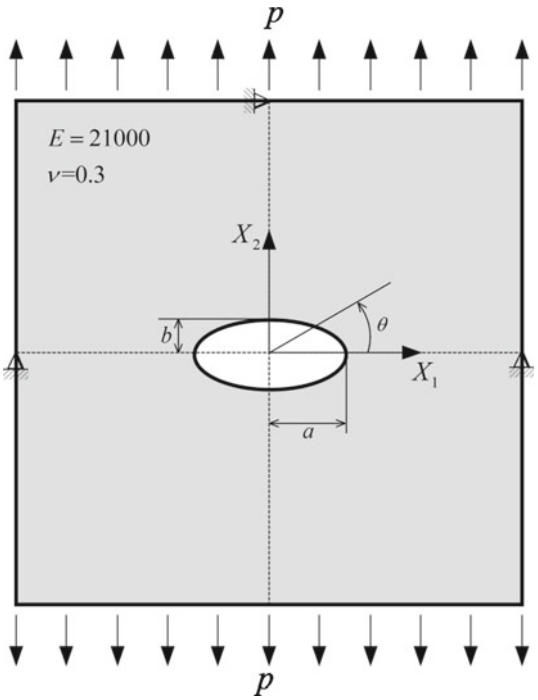

Fig. 5 *Square* plate with a centered *elliptical hole* under tension

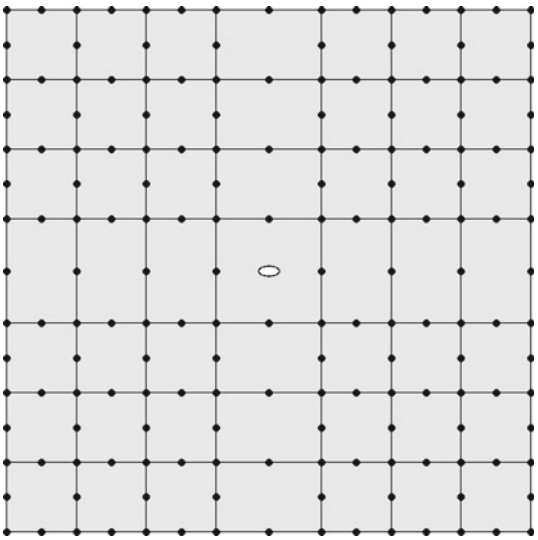

Fig. 6 Mesh configuration of special element

4.2 Infinite plate with an inclined elliptical hole under tension

The second example considered is an infinite plate containing an inclined elliptical hole and subjected to uniform tension along the vertical direction. The inclined angle of the elliptical hole to the horizontal axis is defined as α (see Fig. 11). The analytical solutions can be derived using two complex potential functions given in [17] and proper coordinate transformation.

The size of the solution domain is selected to be the same as the square plate used in Example 1, and the corresponding hybrid finite element discretization is shown in Fig. 12, in which $\alpha = 30^{\circ}, 45^{\circ}, 60^{\circ}, 90^{\circ}$ are considered. The mesh configuration for the case of $\alpha = 0^{\circ}$ is the same as that in Example 1. The ratio a/b is set to be 2. To perform hybrid finite element analysis, the necessary displacement constraints should be introduced into the stiffness equation to remove the singularity of the stiffness matrix. For this purpose, the

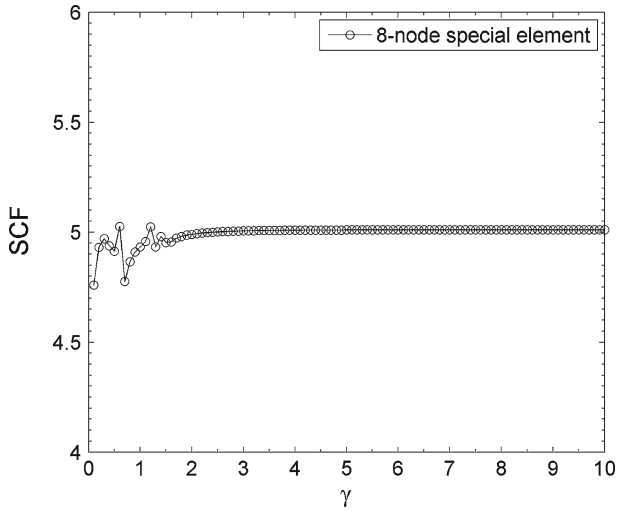

Fig. 7 Effect of the location of source points outside the element domain

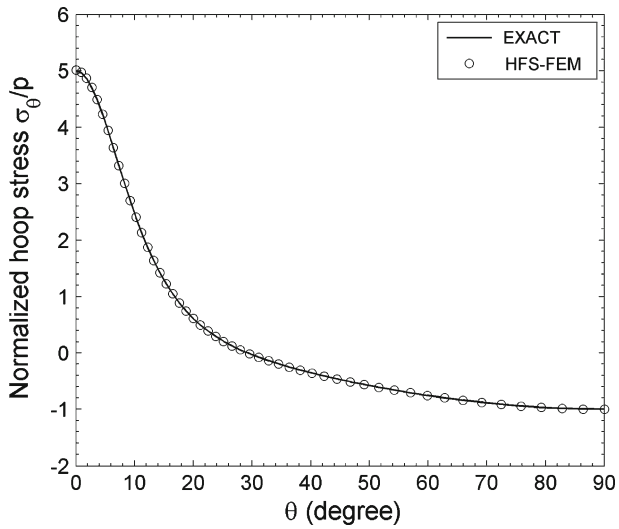

Fig. 8 Variation of hoop stress along the boundary of *elliptical hole*

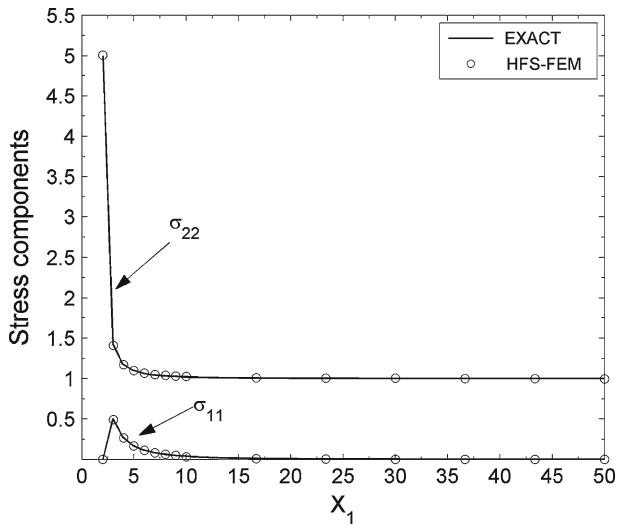

Fig. 9 Stress decay along the *horizontal* coordinate axis

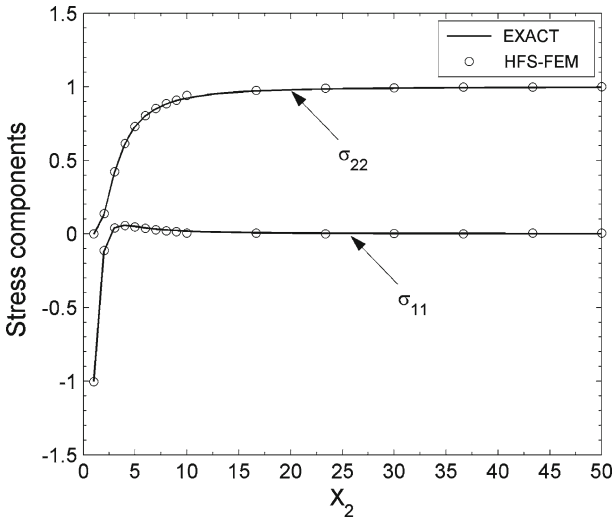

Fig. 10 Stress decay along the vertical coordinate axis

Table 1 Stress concentration factor for various ratios of *a/b*

a/*b*	1	2	3	4	5	6	7	8
Exact	3	5	7	9	11	13	15	17
HFS-FEM	3.008	5.010	7.012	9.015	11.018	13.021	15.024	17.026
Percentage relative error (%)	0.27	0.20	0.17	0.17	0.16	0.16	0.16	0.15

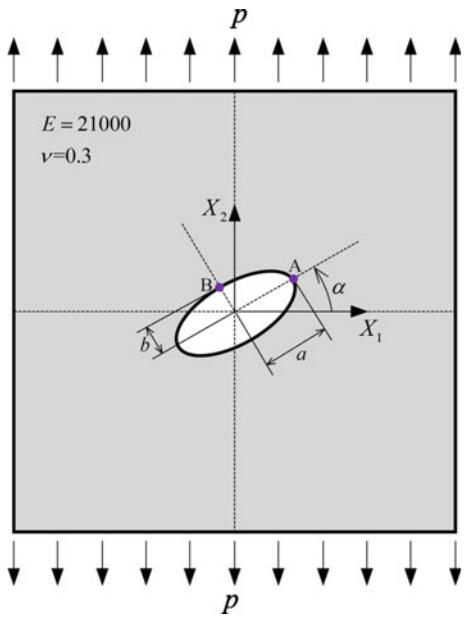

Fig. 11 *Square* plate with an inclined *elliptical hole* under tension

analytical displacement solutions at points (−50, 50), (50,50) and (50, −50) are calculated and applied during the procedure of hybrid finite element analysis.

The stress concentration coefficients at points *A* and *B* are studied and presented in Fig. 13 as a function of the inclination angle α. From Fig. 13 it can be seen that the numerical results agree well with the analytical solutions. The good agreement demonstrates the accuracy of the present hybrid finite element formulation and special elliptical-hole element. More importantly, the mesh used in the present approach is relatively simpler. The number of elements used for various inclination angles is 35, 38, 38 and 49, respectively, and the corresponding number of nodes is 130, 139, 139 and 176, respectively.

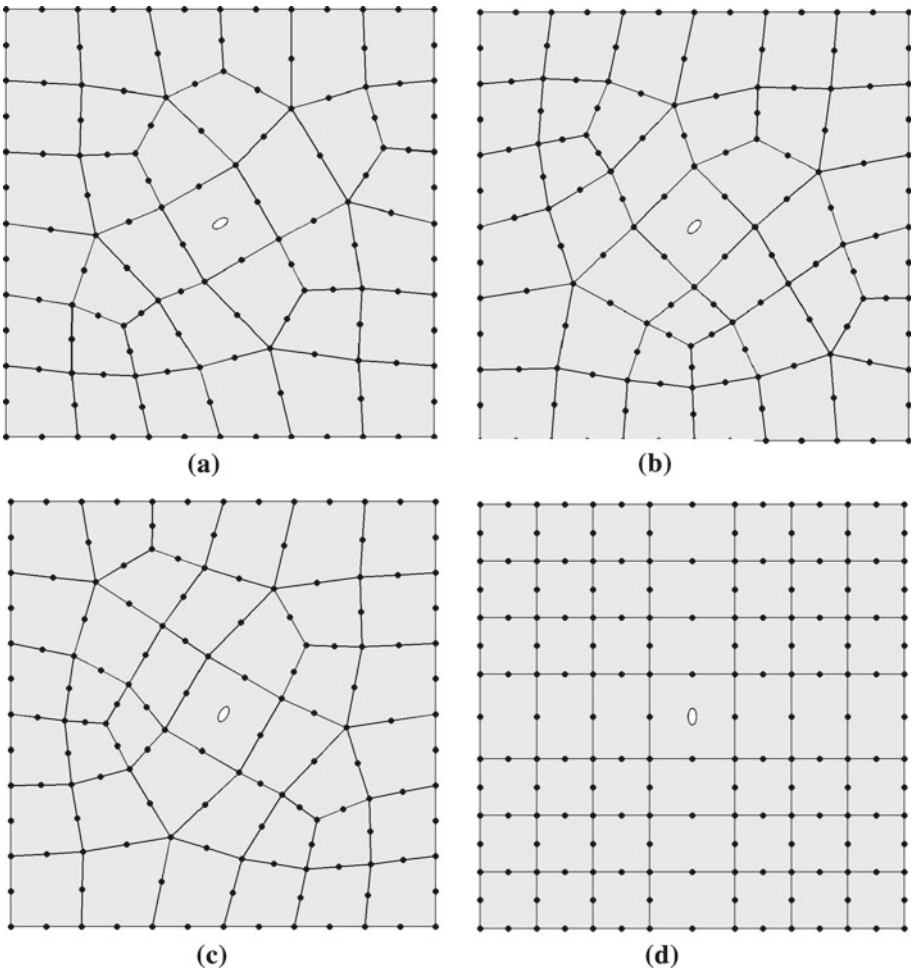

Fig. 12 Mesh configurations for the inclined *elliptical hole*. **a** $\alpha = 30°$, **b** $\alpha = 45°$, **c** $\alpha = 60°$, **d** $\alpha = 90°$

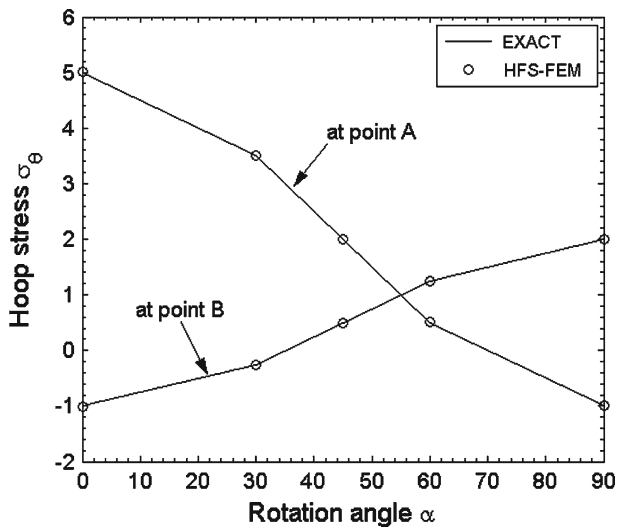

Fig. 13 Variation of hoop stress for different rotation angles of the elliptical hole

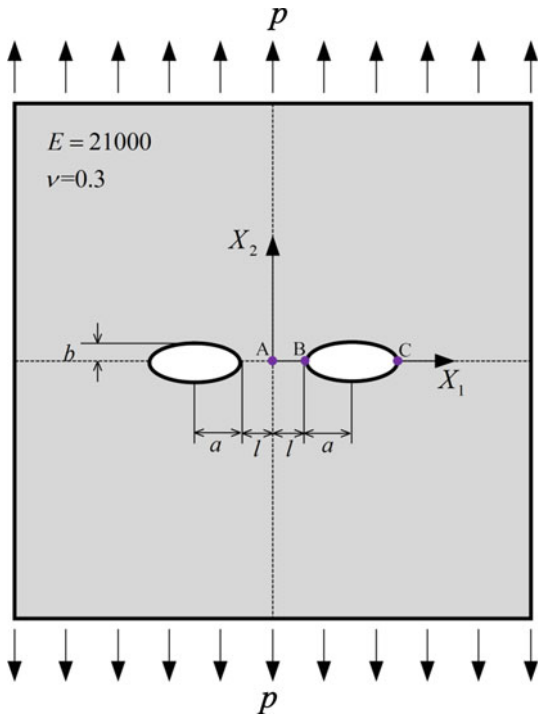

Fig. 14 Infinite plate containing two *elliptical holes* under uniaxial tension

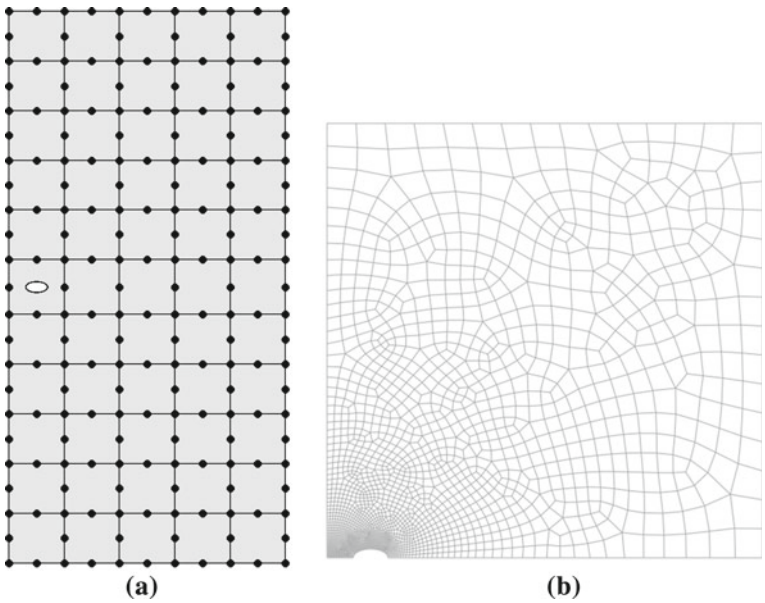

Fig. 15 **a** Hybrid finite element grid with one 8-node special element. **b** Conventional finite element grid for $l = 3$

4.3 Interaction of two elliptical holes under tension

This example is used to investigate the interaction of two elliptical holes, as displayed in Fig. 14. The plate is modeled with a finite size of 100 $\times$ 100, and the two elliptical holes have same shape, with major axis $2a = 4$ and minor axis $2b = 2$. The distance between these two holes is denoted by l.

When the distance parameter $l = 3$, only half of the domain is modeled due to the symmetry of the problem, and the hybrid finite element division with one 8-node special element is plotted in Fig. 15, in which the conventional finite element grid of the representative quarter of the domain is generated using ABAQUS for

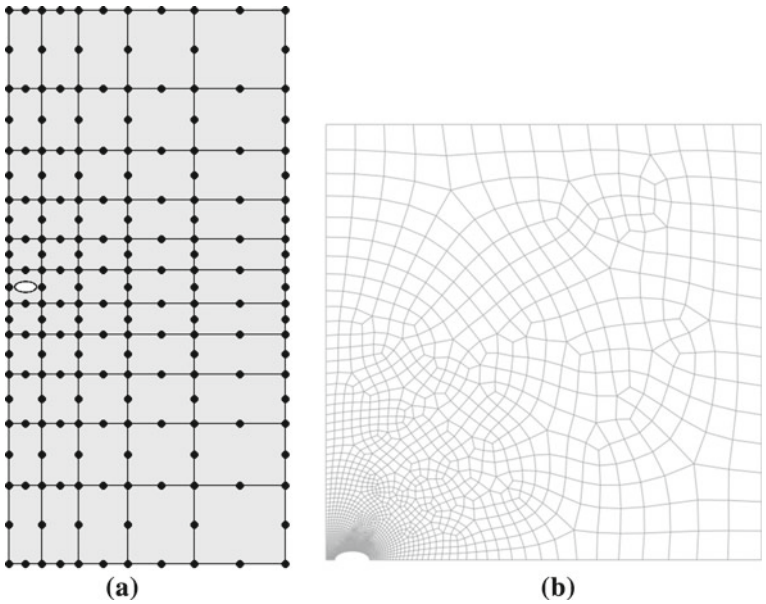

Fig. 16 **a** Hybrid finite element grid with one 8-node special element. **b** Conventional finite element grid for $l = 1$

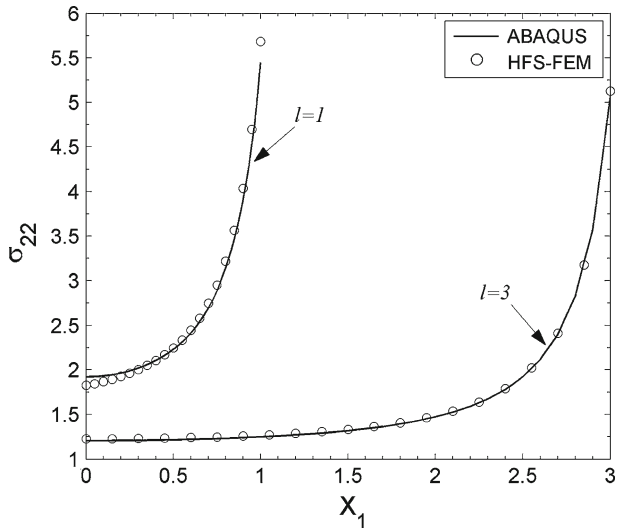

Fig. 17 Stress variation along the horizontal axis between the two elliptical holes with 8-node special element

the purpose of comparison. In the present hybrid finite element grid, a total of 55 quadratic hybrid elements with 198 nodes are used, whereas the conventional finite element grid uses 2,786 elements of the type CPS8R including 8,569 nodes in ABAQUS. Also, Fig. 16 displays the corresponding finite element grids of the present model and the conventional finite element model for the case of $l = 1$. The results in Fig. 17 give the variation of stress component σ_{22} between the two elliptical holes, and it can be seen that there is a significant increase in the maximum value of stress as the distance parameter l decreases. The main reason is that the interaction of two elliptical holes becomes stronger as the two elliptical holes come closer. For the case of $l = 3$, the present 8-node special element can well capture the variation of stress σ_{22}, and good agreement is observed between the results of the present HFS-FEM and that from ABAQUS. The maximum relative error between the two methods is 1.223 % at the left point B of the elliptical hole. In this case, the stress concentration factor at the right point C of the elliptical hole is 5.078, which is very close to the theoretical value of a single elliptical hole in an infinite plane, as described in Example 1. For the case $l = 1$, the stress concentration factor at the point B obtained using the present hybrid model reaches 5.682 and has a large discrepancy against the results of

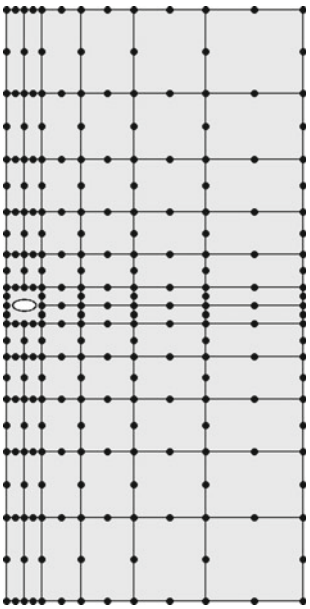

Fig. 18 Hybrid finite element grid with one 16-node special element

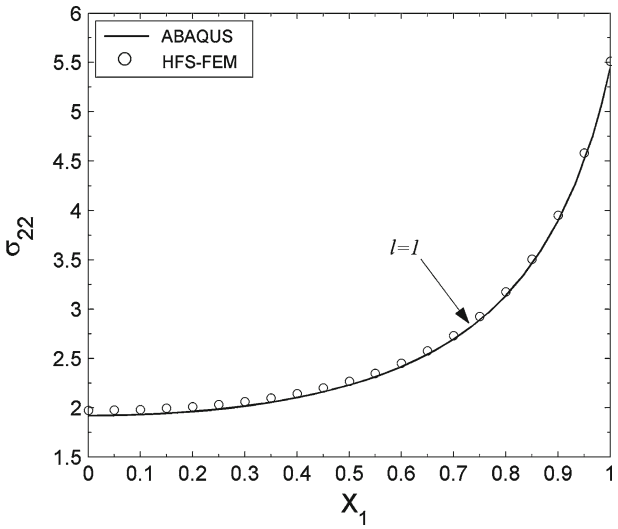

Fig. 19 Stress variation along the horizontal axis between the two elliptical holes with 16-node special element

Table 2 Stress σ_{22} at three points for the case of $l = 1$

	A	*B*	*C*
HFS-FEM			
8-node special element	1.827	5.682	5.395
16-node special element	1.973	5.512	5.201
ABAQUS	1.919	5.446	5.162

ABAQUS, which use 2,109 elements and 6,528 nodes. Thus, the present 8-nodel special element is inadequate to capture the strong interaction of two elliptical holes.

To deal with the strong interaction of two elliptical holes, the 16-node special element shown in Fig. 4b is employed here and the corresponding mesh grid is displayed in Fig. 18. The stress results in Fig. 19 show that the 16-node special elliptical-hole element can give better accuracy than the 8-node special element.

Finally, the stress results at points *A*, *B* and *C* displayed in Fig. 14 are tabulated in Table 2.

5 Conclusions

A special-fundamental-solution-based finite element formulation is established to provide an efficient approach for stress concentration analysis around elliptical holes, in which the special fundamental solutions associated with the elliptical hole are used to approximate the element's interior displacement and stress fields, and the shape functions used in the conventional FEM and BEM are employed for the element frame displacement fields. Due to the properties of special fundamental solutions, the special element is designed to enclose an elliptical hole and thus the local mesh refinement around the elliptical hole is avoided. The special hybrid elements developed may have different numbers of nodes with quadratically varying displacement approximation along their boundary to match with complex surrounding geometry. Numerical results from three examples, namely a square domain with a horizontal elliptical hole, an inclined elliptical hole, and two elliptical holes, showed that the present special elliptical-hole element can effectively capture the dramatic variation of stress around elliptical holes by using relatively coarse meshes, whereby the computational cost is significantly reduced. Hence, the present approach can be employed to effectively predict the stress concentration factor associated with elliptical holes.

Acknowledgments The research in this paper is partially supported by the Natural Science Foundation of China under the grant no. 11102059.

References

1. Chau, K.T., Wang, Y.B.: A new boundary integral formulation for plane elastic bodies containing cracks and holes. Int. J. Solids Struct. **36**(14), 2041–2074 (1999)
2. Denda, M., Kosaka, I.: Dislocation and point-force-based approach to the special Green's Function BEM for elliptic hole and crack problems in two dimensions. Int. J. Numer. Methods Eng. **40**(15), 2857–2889 (1997)
3. Clements, D.L., Haselgrove, M.D.: A boundary integral equation method for a class of crack problems in anisotropic elasticity. Int. J. Comput. Math. **12**(3–4), 267–278 (1983)
4. Ang, W.T., Clements, D.L.: A boundary element method for determining the effect of holes on the stress distribution around a crack. Int. J. Numer. Methods Eng. **23**(9), 1727–1737 (1986)
5. Kamel, M., Liaw, B.M.: Boundary element formulation with special kernels for an anisotropic plate containing an elliptical hole or a crack. Eng. Fract. Mech. **39**(4), 695–711 (1991)
6. Qin, Q.H., Mai, Y.W.: BEM for crack-hole problems in thermopiezoelectric materials. Eng. Fract. Mech. **69**(5), 577–588 (2002)
7. Hwu, C., Liao, C.Y.: A special boundary element for the problems of multi-holes, cracks and inclusions. Comput. Struct. **51**(1), 23–31 (1994)
8. Ting, K., Chen, K.T., Yang, W.S.: Boundary element alternating method applied to analyze the stress concentration problems of multiple elliptical holes in an infinite domain. Nucl. Eng. Des. **187**(3), 303–313 (1999)
9. Piltner, R.: Special finite elements with holes and internal cracks. Int. J. Numer. Methods Eng. **21**(8), 1471–1485 (1985)
10. Dhanasekar, M., Han, J.J., Qin, Q.H.: A hybrid-Trefftz element containing an elliptic hole. Finite Elem. Anal. Des. **42**(14–15), 1314–1323 (2006)
11. Qin, Q.H.: The Trefftz Finite and Boundary Element Method. WIT Press, Southampton (2000)
12. Wang, H., Qin, Q.H.: Hybrid FEM with fundamental solutions as trial functions for heat conduction simulation. Acta Mech. Solida Sin. **22**(5), 487–498 (2009)
13. Wang, H., Qin, Q.H.: Special fiber elements for thermal analysis of fiber-reinforced composites. Eng. Comput. **28**(8), 1079–1097 (2011)
14. Wang, H., Qin, Q.H.: Fundamental-solution-based hybrid FEM for plane elasticity with special elements. Comput. Mech. **48**(5), 515–528 (2011)
15. Wang, H., Qin, Q.H.: Fundamental-solution-based finite element model for plane orthotropic elastic bodies. Eur. J. Mech. A Solids **29**(5), 801–809 (2010)
16. Qin, Q.H.: Trefftz finite element method and its applications. Appl. Mech. Rev. **58**(5), 316–337 (2005)
17. Muskhelishvili, N.I.: Some Basic Problems of the Mathematical Theory of Elasticity. Noordhoff Ltd., Groningen (1953)
18. Wang, H., Qin, Q.H., Kang, Y.L.: A new meshless method for steady-state heat conduction problems in anisotropic and inhomogeneous media. Arch. Appl. Mech. **74**(8), 563–579 (2005)
19. Wang, H., Qin, Q.H.: Meshless approach for thermo-mechanical analysis of functionally graded materials. Eng. Anal. Boundary Elem. **32**, 704–712 (2008)
20. Wang, H., Qin, Q.H.: Some problems with the method of fundamental solution using radial basis functions. Acta Mech. Solida Sin. **20**(1), 21–29 (2007)
21. Qin, Q.H., Wang, H.: Matlab and C Programming for Trefftz Finite Element Methods. CRC Press, Boca Raton (2009)
22. Piltner, R.: Some remarks on finite elements with an elliptic hole. Finite Elem. Anal. Des. **44**(12–13), 767–772 (2008)